Hindawi
International Journal of Energy Research
Volume 2023, Article ID 6919663, 18 pages
https://doi.org/10.1155/2023/6919663

Research Article

Toward Commercialization of Mechanical Energy Harvester: Reusable Triboelectric Nanogenerator Based on Closed-Loop Mass Production of Recyclable Thermoplastic Fluoropolymer with Microstructures

Yoonsang Ra,[1] Jong Hyun Lee,[2] Jiho Bang,[1] Donghan Lee,[1] Dongik Kam,[1] Sumin Cho,[1] Sunmin Jang,[1] Donghyeon Yoo,[3,4] Jong Woo Kim,[1] Kyoung Je Cha,[2] and Dongwhi Choi[1]

[1]*Department of Mechanical Engineering (Integrated Engineering Program), Kyung Hee University, 1732 Deogyeong-daero, Yongin, Gyeonggi 17104, Republic of Korea*
[2]*Smart Manufacturing Technology R&D Group, Korea Institute of Industrial Technology, Techno Sunhwan-ro 320, Daegu 31056, Republic of Korea*
[3]*Department of Mechanical Engineering, Pohang University of Science and Technology (POSTECH), 77 Cheongam-ro, Pohang, Gyeongbuk 37673, Republic of Korea*
[4]*Department of Mechanical Science and Engineering, University of Illinois Urbana-Champaign, Urbana, IL 61801, USA*

Correspondence should be addressed to Kyoung Je Cha; kjcha@kitech.re.kr and Dongwhi Choi; dongwhi.choi@khu.ac.kr

Received 22 May 2023; Revised 4 July 2023; Accepted 19 October 2023; Published 22 November 2023

Academic Editor: Arun Thirumurugan

Copyright © 2023 Yoonsang Ra et al. This is an open access article distributed under the Creative Commons Attribution License, which permits unrestricted use, distribution, and reproduction in any medium, provided the original work is properly cited.

Triboelectric nanogenerators (TENGs) have been considered a promising energy harvester. However, the wear-induced limited lifetime of the surface structure on fluoropolymeric contact layers of the TENG has been a critical issue in its commercialization because surface structures on soft engineering materials play a key role in enhancing the generation of electricity in TENGs. After the surface structure on the polymeric contact layer is worn out, the layer is required to be replaced with a new one with intact surface structures to reenhance the degraded output performance of the TENG. Herein, injection molding-assisted mass production is applied to manufacture micro/nanoscale surface-structured perfluoroalkoxy alkane (PFA) contact layers, which exhibit easily replaceable but fully recyclable characteristics. The optimized production time is shorter than 1 min, and the unit cost under $1 of manufacturing surface-structured PFA contact layers is achieved. TENG with the fabricated PFA contact layer can generate over 620 V of voltage and up to 12.4 mW of power from solid-solid contact and separation when the contact area is 5 cm × 5 cm and the contact frequency is 10 Hz. The manufactured PFA contact layer can be facilely replaced with a new one before the end of its lifetime to maintain the electrical output of the TENG, and the postused one can be fully recycled via reprocessing as the material for injection molding. Consequently, a tile-floor-based TENG is proposed as a proof-of-concept demonstration to show environmentally friendly and closed-loop production of TENGs.

1. Introduction

As portable/wearable electronic technology has rapidly developed and human lifestyle has moved toward the epoch of the Internet of Things, the issue of power supply to electronic devices has emerged [1, 2]. Energy harvesting technology, which can offset energy consumption and complement equipped batteries, is considered a favorable solution for powering various portable/wearable devices with elongated operation durations [3–5]. Thus, various energy harvesting devices, such as electromagnetic generators [6, 7], piezoelectric nanogenerators [8], and triboelectric nanogenerators (TENGs)

[9–11], are being investigated by numerous research groups. TENGs are highlighted as one of the most promising energy harvesters due to their unique advantages, such as their facile working mechanism and extremely diverse material choice [12–19]. The fundamental principle of TENGs is the triboelectric effect (also called contact electrification), which spontaneously occurs with the physical contact of surfaces of different materials. In this regard, it is well known that the difference in the work function of the contacted two materials can affect the triboelectric effect. Among various engineering materials, fluoropolymeric materials have been verified as one of the most proper materials for contact layers of TENGs owing to their advantageous electrical characteristics that can easily generate a considerable amount of static charge on the surface through contact with other materials and can hold the surface charges for a long time due to their excellent dielectric properties.

As with other energy harvesting devices, enhancing output performance is one of the most critical issues in the field of TENGs [20–24]. Among various strategies to elevate the electrical output of TENGs, the fabrication of micro/nanoscale structures on the fluoropolymeric contact layer has been frequently proposed by numerous literatures as one of the most effective strategies [9, 25–29]. However, the durability of micro/nanoscale structures on the most widely utilized fluoropolymeric contact layer of the TENG becomes a problem since polymers are considered relatively soft engineering materials. Given that TENGs are operated on the basis of sequential contact and separation of two materials, the wear of the structures on the contact surface, which directly degrades the performance of TENGs, is inevitable; thus, the wear issue of surface structures on such polymeric contact layers has become a major hurdle for TENGs for their commercialization [9, 30–32]. In order to reenhance the degraded output performance after the surface structure is worn out, the contact layer is required to be replaced with a new one with an intact surface structure. However, such frequent replacement of the fluoropolymeric contact layer of TENG may cause environmentally unfriendly problems such as the generation of a large amount of poorly decomposed plastic wastes, and thus, it is necessary to propose an appropriate approach to face this problem as one step forward to the commercialization of TENG.

In this study, a micro/nanoscale structured thermoplastic fluoropolymer contact layer produced by a one-step rapid process based on injection molding is proposed for practical TENGs, which can be utilized as ecofriendly energy harvesters on the basis of the replaceable but fully recyclable zero-waste contact layer. Inexpensive mass production has been the main driving force behind the commercialization and popularization of most existing polymeric products since cost-effective, large-quantitative, and reliable qualitative production can help polymeric products be available and easily replaceable. Among various manufacturing technologies, injection molding, a manufacturing process in which molten polymer is injected into a mold cavity and solidified to produce a part, is one of the most important methods for effective mass production because of its superior advantages, such as economic feasibility, high manufacturing speed, and reliable mass productivity. The quantitatively and qualitatively reliable mass producibility of the injection molding process can result in easily and fully replaceable TENG contact layers when they reach the end of their useful life and involve significant degradation of the electrical output performance of TENG. On top of that, the injection molding process can be expected to act as the heart of environmentally friendly, closed-loop production of polymeric contact layers, considering that the material used for the contact layer of TENGs in this study is thermoplastic, which is fully recyclable. Additionally, given that the biomaterials are also highlighted for the contact layer of TENG, the future scope of application can be expanded to biorelated fields with the study of injection molding-based manufacturing of biobased materials.

2. Materials and Methods

2.1. Fabrication of the Mold Insert Blocks. NKA80 plastic mold steel was used as the material for the mold insert blocks. The surface of the mold insert block was polished to reduce surface roughness before surface structure fabrication. Then, two methods, i.e., laser machining and electroforming, were applied to fabricate the surface structures. In laser machining, a Ti : sapphire femtosecond (fs) laser system was used to directly fabricate negative structures. The laser produced pulses of 33.5 fs with a maximum energy of 1.2 mJ at a central wavelength of 800 nm with a repetition rate of 5 kHz. Negative microcone structures with a depth of 1.5 μm were fabricated using circularly polarized fs laser pulses (pulse energy of 0.8 μJ, scanning speed of 10 mm/s, and scanning distance of 5 μm). On the other hand, in the case of the electroforming process, the negative structures were fabricated by combining diamond turning machining (DTM). Microscale machining of copper plates with a positive micropyramid (width: 50 μm, length: 50 μm, and height: 40 μm) and micropillar (width, length, distance, and height: 30 μm) was performed on an ultraprecision planning machine, i.e., NIC-300 (Nagase Integrex Co., Ltd.). Copper plates with an area of 6 cm × 6 cm and a thickness of 3 mm were used for the workpieces of the DTM process. The cutting conditions were kept constant at a cut depth of 10 μm, a cutting speed of 1 m/min, and a feed rate of 15 μm/rev. Then, the patterned surface of copper plates was passivated with potassium dichromate to build a separation layer. The electroforming process of the machined copper plates, which were used as cathode material, was then conducted in a nickel sulfamate bath until the nickel layer was 2 mm thick. Bath temperature and current density were controlled for the high deposition rate and low internal stress of electroformed nickel plates. The electroformed nickel plates with negative patterns A and B were detached from the copper plates and then cut into 3 cm × 3 cm and 5 cm × 5 cm sizes. Finally, nickel mold inserts were obtained by welding the cut nickel plates to the mold insert blocks.

2.2. Surface Topography Investigation Methods. The surface topography of the fabricated mold inserts and the replicated perfluoroalkoxy alkane (PFA) contact layers was investigated using an optical microscope (VHX-950F, KEYENCE, Osaka, Japan), a 3D laser confocal microscope (Olympus; OLS4100), and a field-emission scanning electron microscopy (FE-SEM; JEOL JSM-7900F). A contact angle meter (SmartDrop_Plus, Femtobiomed, Korea) was used to measure the contact angle,

which represents the hydrophobicity of the surface. A total of 10 μL of a deionized water droplet was gently placed on the surface, and then the contact angle was measured.

2.3. Electrical Characterization of the TENG. TENG with the PFA contact layer included the aluminum layer (electrode), 3-aminopropyltriethoxysilane (APTES) layer (counter layer), and polymethylmethacrylate (PMMA) layer (substrate). A mechanical shaker (ET-139, Labworks Inc., Costa Mesa, CA, USA) with a connected amplifier (PA-138, Labworks Inc., Costa Mesa, CA, USA) and function generator (DZ1022Z, Rigol, Beaverton, OR, USA) was used to make the uniform vibration to operate the fabricated solid-solid contact-based TENG systematically and for conducting parametric studies including electrical output characterization. For the experiments to characterize the electrical output performance of liquid-solid contact-based TENG, the deionized water droplets with 20 mL of volume were configurated by a syringe pump (NE-4000, New Era Pump Systems, Farmingdale, NY, USA) and dropped from 50 cm of height to the PFA contact layer. Voltage was measured by an oscilloscope (DS1074z, Rigol, Beaverton, OR, USA, internal resistance = 1 MΩ) and a high-voltage probe (DP-22Kpro, PINTEK, Taiwan, internal resistance = 100 MΩ). All experiments related to electrical energy output were conducted at $24 \pm 0.5^{\circ}$C and a relative humidity of 50%.

3. Results and Discussion

3.1. Injection Molding Process to Manufacture Fluoropolymeric Contact Layers of TENGs. The injection molding process consists of mold closing, injection, cooling, and ejection, as shown in Figure 1. In detail, the process starts with mold closing and is followed by the injection of the molten material into the mold. After the mold cavity is filled, the molten material is solidified by cooling. Then, the mold is opened, and the fabricated part is ejected. The typical cycle time is relatively fast, and products with complex shapes can be rapidly produced at a reduced unit cost. Moreover, various materials, such as polymer, elastomer, and metal, can be used in the injection molding process, and the micro/nanoscale surface structures can be facilely controlled and replicated by the mold inserts. On the basis of the injection molding process, polymeric contact layers are manufactured and introduced to TENGs. Injection-molded polymeric contact layers with micro/nanoscale structures on the surface can be reliably mass-produced in various desired sizes and shapes and thus can be availably applied to diverse types of TENGs, especially TENGs with a large area. On top of that, given that the polymeric contact layers of TENGs are generally made of thermoplastics such as fluorinated ethylene propylene (FEP), polytetrafluoroethylene (PTFE), and PFA, the postused polymeric contact layers can be easily reprocessed as material for manufacturing new ones. Such a closed-loop cycle of production and zero-waste manufacturing can play a core role in the ecofriendly industry in the future. Figure 2(a) shows a photograph and schematic of the fabrication process of a negatively surface-structured metallic mold insert, which determines the shape and surface characteristics of the product. The negative surface structure can be fabricated through various metal processing methods, such as machining, electroforming, and forging; but in this work, the structure is directly fabricated by laser machining on the surface of the mold insert block, as shown in the schematic. Figure 2(b) is a photograph of the fabricated mold insert block with microcone-shaped surface structures. Here, the fabrication of the mold insert block, which has microstructures on the surface, is not limited to laser machining, and various methods can be applied. Another fabrication method, as an example, is described in Materials and Methods and Figure S1 in the Supplementary Materials. Figure S1 shows the process for fabricating the mold insert block using diamond turning machining (DTM) and electroforming. A standard side gate mold base (two-plate mold) is designed and fabricated for the injection molding process, as shown in Figures 2(c) and 2(d). A mold insert is placed at the center of the moving part and could be easily changed to another mold insert. A temperature controller with cartridge heaters is used to increase the temperature of the mold insert and mold base. A conventional injection molding machine (WIZ80E; LS Mtron) with a Hastelloy C-276 feed screw in the injection unit is used to fabricate a polymeric contact layer with surface structures through the injection molding of fluoropolymers. Fluoropolymers, which have fluorine- (F-) containing end groups such as FEP, PTFE, and PFA, have been proven to be superior materials for the contact layer of TENGs in terms of generating a high amount of negative electric charges via contact with other materials [33–37]. However, injection molding of fluoropolymers has limitations due to their shear sensitivity, high melt temperature, and generation of corrosive fluorine gas [38–40]. In this respect, the Hastelloy feed screw, which is a highly corrosion-resistant nickel alloy, is introduced into the injection unit for flowing material at temperatures above the melting point and preventing the corrosion caused by fluorine gas during the injection molding process. Furthermore, the processing conditions for mass production of polymeric contact layers with surface structures are designed on the basis of the Taguchi method, and the core parameters, such as mold temperature, injection speed, packing pressure, and packing time, are optimized to increase the replication quality of the contact layer and its surface structure, as shown in Figure 2(e). Figure S2 in the Supplementary Materials shows the change in the surface topography of the injection-molded PFA contact layers and the S/N ratio in the optimization of the injection molding process. The experimental parameter design for the injection molding process is shown in Tables S1 and S2 in the Supplementary Materials. Table S1 shows levels of the parameters including the mold temperature, the injection speed, the packing pressure, and the packing time. Table S2 shows the experiment number and the orthogonal arrays of $L_9 3^4$. Details of the optimization process are described in the Supplementary Materials, and the optimized processing parameters and conditions applied to the injection molding process for the replication of PFA contact layers are shown in Table S3 in the Supplementary Materials. In the method described, the PFA contact layer is mass-produced with rapid speed and reliable quality. The production time and unit cost for each contact layer are less than 1 min and under $1,

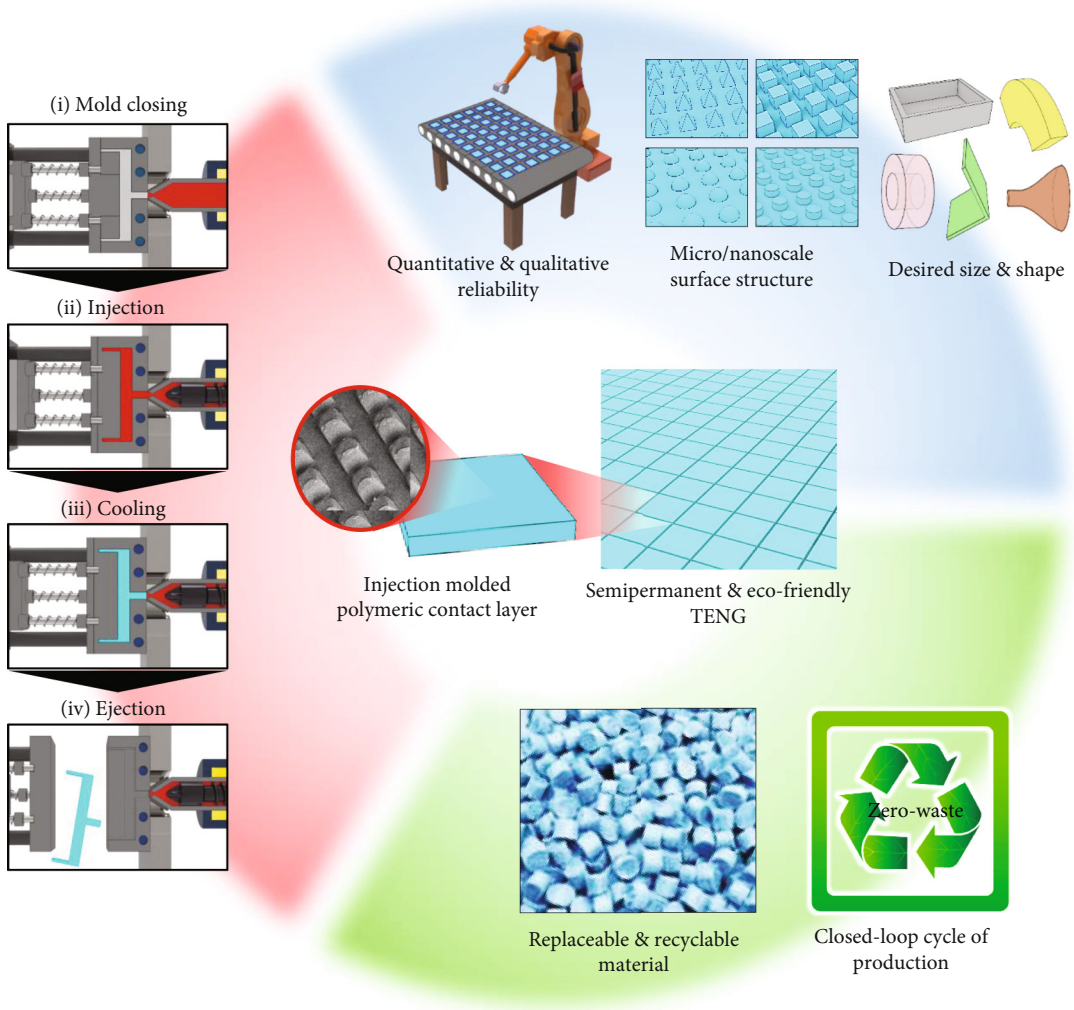

Figure 1: Process of the injection molding process and advantages when the injection-molded polymeric contact layer is introduced to TENG.

respectively, considering the mold insert manufacturing cost, injection molding process cost, and material cost under the optimized process condition, as shown in Table S4. In addition, monthly production costs, including labor and other incidental costs (e.g., electricity usage), are calculated in consideration of production capacity (see Table S4 in the Supplementary Materials). Moreover, a conveyor system as well as a robot arm for the automatic manufacturing of such a contact layer are introduced. Figure 2(f) shows the mass producibility of PFA contact layers through the injection molding process, which can produce more than 70 contact layers in 1 h. Figures 2(g) and 2(h) show photographs and SEM images of the various sizes and surface structures of the fabricated PFA contact layer. The scale and surface structure of polymeric contact layers can be facilely controlled by changing the mold insert. Many studies have reported that the output of TENGs varies on the basis of the conditions of the surface structure, e.g., type, height, bottom dimension, and distance between the structures. However, different studies suggest various optimal structures [41–44]. Given that, the optimal condition of the surface structure on contact layers can vary on the basis of different factors, such as the characteristics of the mechanical input energy, the design and working mode of the TENG, and environmental conditions. In this respect, injection molding-based manufacturing of polymeric contact layers can be an integrated solution that can versatilely cope with the changes in diverse requirements. Photographs and the surface topographies of the mold inserts including three types of negative surface structures (microcone shape, microsquare pillar shape, and microsquare pyramid shape) are shown in Figure S3 in the Supplementary Materials. PFA contact layers can be mass-produced at low cost and high speed, and moreover, their size and surface structures can be easily controlled in the injection molding process by changing the mold insert block.

3.2. Electrical Output Characteristics of Solid-Solid Contact-Based TENGs with Injection-Molded PFA Contact Layers. A schematic and the working mechanism of a solid-solid contact-based TENG (S-S TENG) with an injection-molded

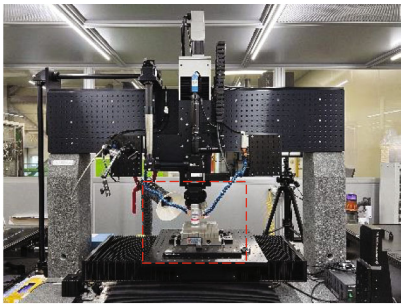

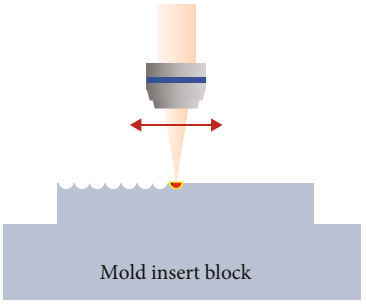

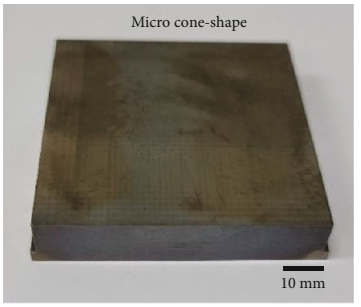

(a) (b)

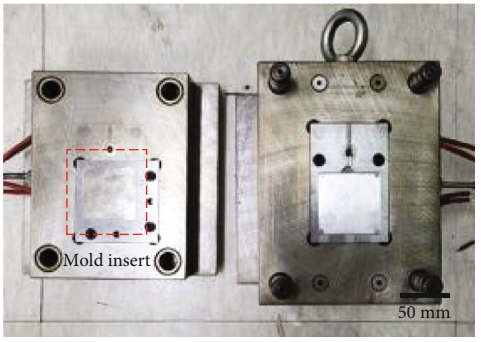

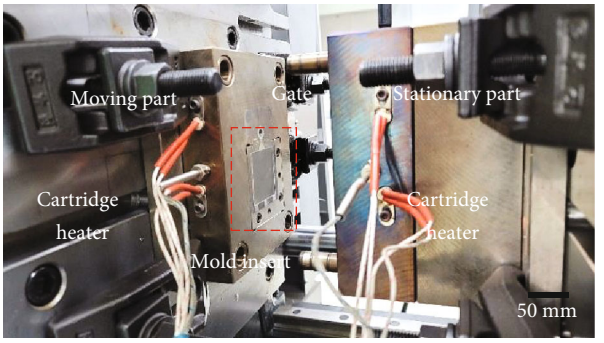

(c) (d)

(e)

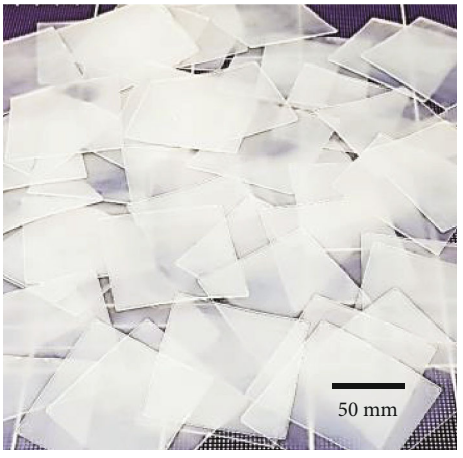

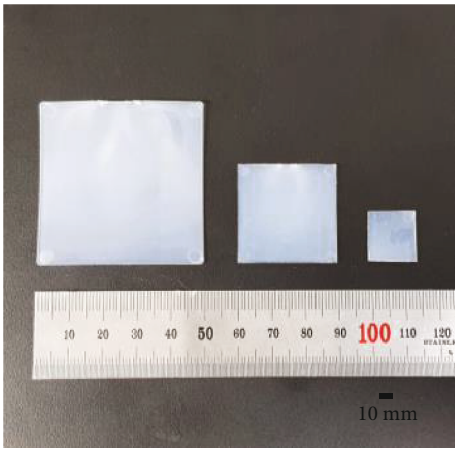

(f) (g)

Figure 2: Continued.

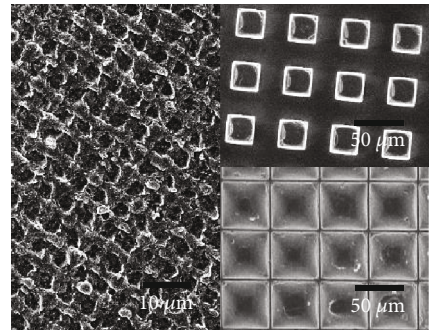

(h)

Figure 2: (a) Fabrication of the negative surface-structured metallic mold insert and (b) photograph of the fabricated mold insert block. (c) Mounting of the mold inserts on the moving part of the injection molding machine. (d) Clamping unit and molding part of the injection molding machine. (e) Fabricated PFA contact layers undergoing short-shot testing of the manufacturing process. (f) Mass producibility of the injection-molded PFA contact layer. (g) Photograph of the various sizes of the fabricated PFA contact layers. (h) SEM images of various surface structures of the fabricated PFA contact layers.

PFA contact layer are illustrated in Figure 3(a). For measuring the output voltage, an oscilloscope and high-voltage probe are used in every following experiment. The upper left inset circuit diagram in Figure 3(a) shows the connection way of the oscilloscope and high-voltage probe to TENG schematically. The load resistances of the oscilloscope and the high-voltage probe are 1 and 100 MΩ, respectively. As mentioned above, electrical output is generated on the basis of the sequential contact and separation of the contact and counter layers. In this regard, the mechanical shaker, which can make uniform vibrations based on a connected function generator, is used for systematic experiments, as shown in Figure S4 in the Supplementary Materials. Figure S4(a) is the photograph of the experimental setup for the operation of S-S TENG, and Figure S4(b) shows the PFA contact layer and APTES counter layer, which are attached to the electrodes, and how they are mounted on the shaker. The PMMA plates are used as the substrate for holding the layers. A raw data graph of the output voltage (defined as V_O in this study), which is measured using an oscilloscope, generated by an S-S TENG with a microcone-shape structured PFA contact layer when the size of the contact area is 5 cm × 5 cm and the contact frequency is 10 Hz, is representatively plotted in Figure 3(b). V_O can be measured as a form of a peak surging at the moments of contact and separation. The output performance of S-S TENG is continuously measured from before its operation until the electrical output is saturated to confirm the gradual increase and saturation of the electrical output of TENG with its continuous operation based on the increase in the charging degree of the contact surface. Resultingly, S-S TENG with the fabricated PFA contact layer saturates its electrical output in a very short time after starting up, as shown in Figure S5. To ensure the repeatability of the experimental result, repeated experiments are conducted, as shown in Figures S5(a)–S5(c), and the PFA contact layer is washed before every experiment with isopropyl alcohol to remove surface charges. The change in output performance under different contact frequencies is investigated, as shown in Figure 3(c). V_O should linearly increase as the contact frequency increases on the basis of the working mechanism of the TENG and the voltage measurement principle of the oscilloscope by following the following equations:

$$V_O = I(R_O + R_H),$$
$$I = \frac{dQ}{dt} \propto f, \tag{1}$$

where I, R_O, R_H, Q, t, and f are the current induced by the operation of the TENG, load resistance of the oscilloscope (1 MΩ), load resistance of the high-voltage probe (100 MΩ), induced electrical charges on the contact surface, time length of the contact surfaces are in contact, and contact frequency, respectively. I should linearly increase as f increases under the assumption that Q is identical; Figure 3(c) shows this relationship well. According to the fundamental principle of TENGs (i.e., based on the contact between two surfaces), the size of the contact area S plays an important role in the electrical performance of TENGs, and Q can be expressed as follows on the basis of its definition:

$$Q = \int_S \sigma dS, \tag{2}$$

where σ is the surface charge density. In this regard, the relationship between the average value of the positive max magnitude of V_O ($V_{O,\max}$) and S is investigated, as shown in Figure 3(d). $V_{O,\max}$ of the TENG shows a linearly proportional relationship with S as expected. The result indicates that TENGs with a large area can produce a larger amount of electricity when the other conditions are identical. Given that TENGs can be practically applied as power sources by directly connecting to electronic devices, which may have different internal resistances, the characterization of the output performance depending on the connected external load resistance is required to estimate its ability to supply electrical power through the impedance matching process. Figure 3(e) shows the changing behavior of $V_{O,\max}$ and the

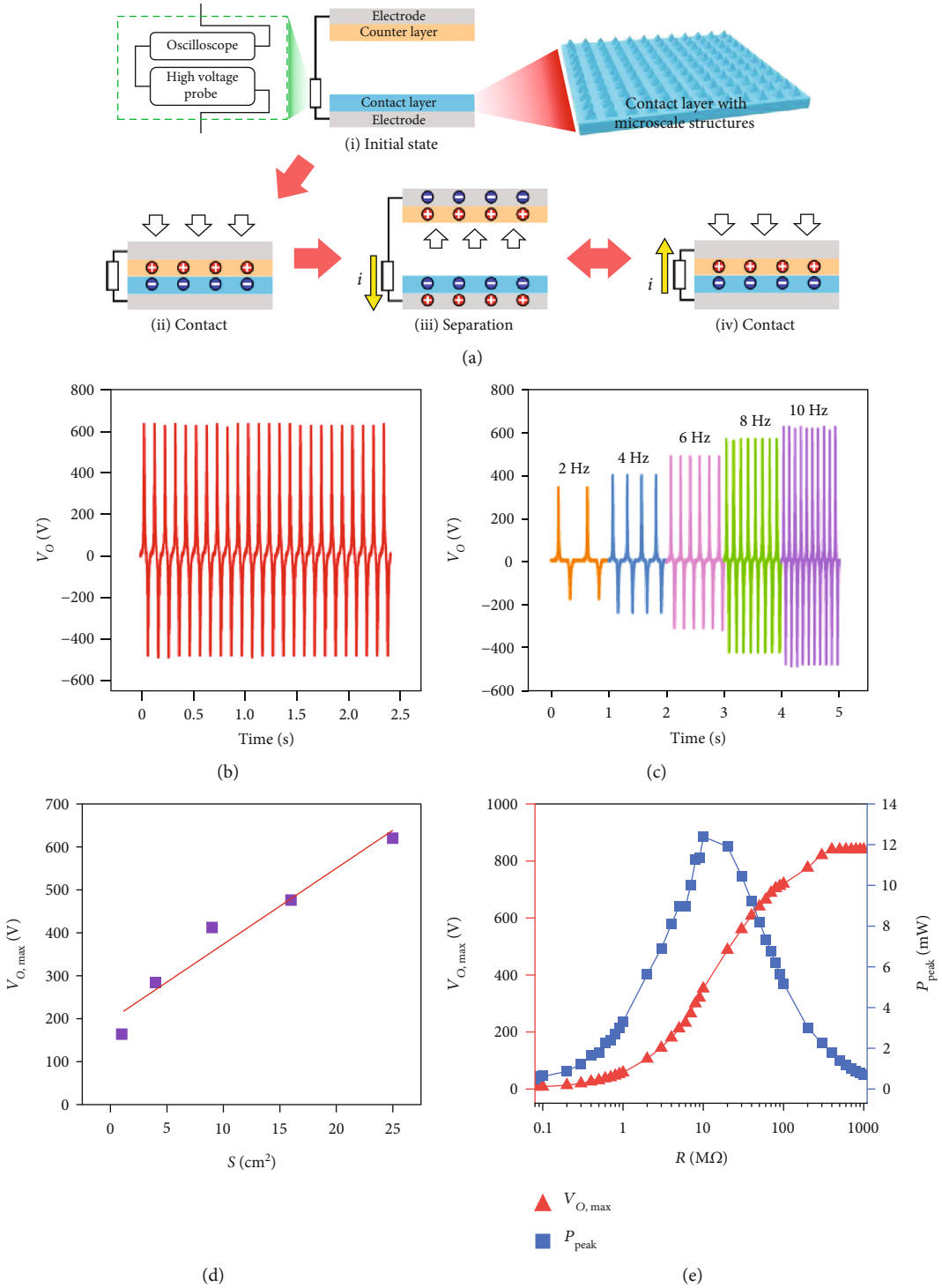

Figure 3: Continued.

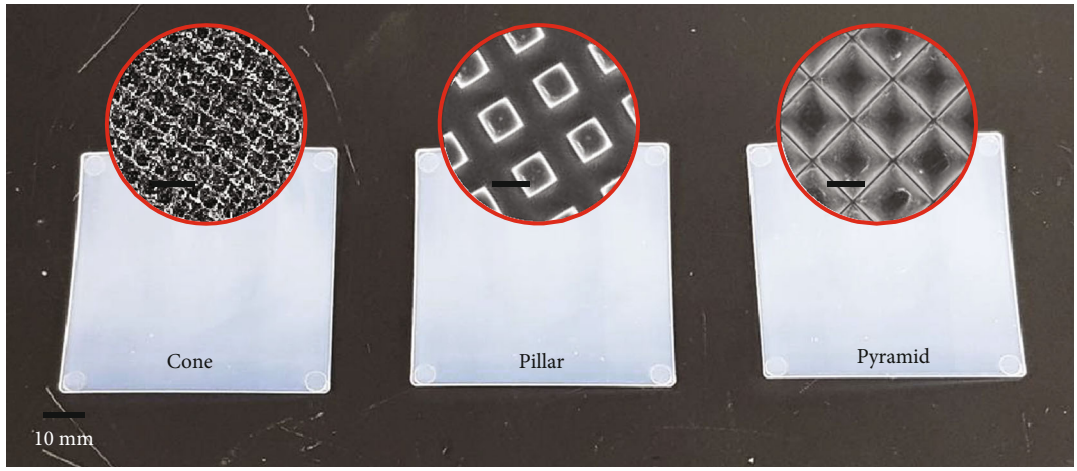

(f)

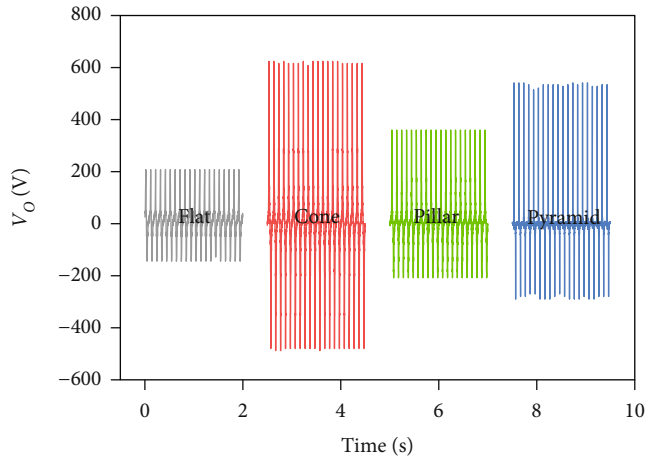

(g)

Figure 3: (a) Schematic and working mechanism of the S-S TENG with the injection-molded polymeric contact layer. The upper left inset circuit diagram is the connection way of the oscilloscope and high-voltage probe to TENG. (b) V_O generated by the S-S TENG with the microcone-shape-structured PFA contact layer and (c) its changing behavior depending on the contact frequency. (d) Variation of $V_{O,\max}$ by varying the contact area. (e) $V_{O,\max}$ and P_{peak} according to the connected external load resistance. (f) Photographs and surface SEM images of the PFA contact layers with different surface structures (microcone shape, microsquare pillar shape, and microsquare pyramid shape, respectively) manufactured by the injection molding process. The scale bars in the SEM images of the microcone shape, microsquare pillar shape, and microsquare pyramid shape are 10, 30, and 30 μm, respectively. (g) The output performances of the TENGs with flat and surface-structured PFA contact layers.

peak electrical power (P_{peak}) by varying the external load resistance. The maximum amount of P_{peak} is 12.4 mW when the connected load resistance is 10 MΩ. The power density is calculated based on the above experimental result and plotted in Figure S6 in the Supplementary Materials. Additionally, all experiments related to electrical energy output are conducted at 24 ± 0.5°C and a relative humidity of 50%. However, the performance of TENG varies significantly with the relative humidity. In this respect, the electrical output performance in the condition of the wide range of relative humidity should be characterized for the commercialization of TENG, and the electrical output of S-S TENG with the injection-molded PFA contact layer according to the relative humidity is suggested, as shown in Figure S7. Figures S8(a) and S8(b) in the Supplementary Materials show the electrical output performances of S-S TENGs with the polylactic acid (PLA) and polyvinyl alcohol (PVA) contact layers, respectively. Bio-based materials are highlighted as one of the most important materials for future TENG due to their various biocompatible functionalities. PLA and PVA are representative bio-based and mass-producible materials. However, such biomaterials are conventionally fluorine-free materials, and this characteristic can be a critical issue in terms of electrical output performance as the presence of fluorine-containing functional groups is known to have a major effect on the electrical output performance of TENG. In this respect, when the injection molding-based manufacturing process of fluorine-contained biomaterials for the contact layer of TENG is developed, the future scope of the application of TENG can be expanded to bio-related fields. Moreover, the expected optimal output behavior of TENGs

depends on their needs. An example is a case where maximum output is instantaneously required when it matters like a sensor for user safety or a case where constant output (even if it is not the maximum output) is reliably required for a long time like a power source at a location that is difficult to reach. In this respect, each TENG is supposed to be designed to generate the required output in accordance with a case. For this reason, the manufacturing of contact layers with surface structures should have a high degree of freedom, reliability, and expansibility of the process. In this respect, the injection molding process has great potential and strengths because it can reliably mass produce the same contact layer with surface structures, and the design of surface structures with a high degree of freedom is relatively facile. Figure 3(f) shows photographs of PFA contact layers manufactured by the injection molding process. The manufactured PFA contact layers have different surface structures in the following shapes: microcone shape, microsquare pillar shape, and microsquare pyramid shape, respectively, and the dimensions of the surface structures are also varied. The insets are the SEM images of each surface. The cone, square pillar, and square pyramid are representative shapes of surface structures, which are reported in various literature for enhancing the electrical output performance of TENG [27]. Moreover, the structures are proper to be manufactured by the one-step process with the injection molding thanks to their shapes that narrow upwards or maintain a constant cross-sectional width. Given that, the contact layers with the three types of surface structures are expected to have advancements in terms of both the manufacturing process and the electrical performance of TENG. Figure 3(g) shows the output performances of TENGs with flat and surface-structured PFA contact layers. TENG with the flat PFA contact layer has the lowest output, and the one with the cone-shaped surface structure has the highest output performance. The experimental results demonstrate that polymeric contact layers with various designs of surface structures can be produced via injection molding, and from that, the output of TENGs can be simply controlled by changing the surface-structured polymeric contact layer in accordance with the needs of users. The PFA contact layer with the cone-shaped surface structure is used to conduct the experiments in Figures 3(b)–3(e).

3.3. Investigation of TENG with Injection-Molded PFA Contact Layer for the Liquid-Solid Contact-Based Environmental Energy Harvesting. As environmental and ecofriendly energy harvesting is highlighted as a promising electrical power supply for a sustainable city, harvesting blue energy is also regarded as one of the bright options. Moreover, many research groups have been reporting the great potential of liquid-solid contact-based TENG (L-S TENG) as a promising energy harvesting technology. Harvesting raindrop energy is expected to be one of the most optimal applications of L-S TENG, and most of the raindrop energy harvesting systems with L-S TENG are introduced outdoors such as the roof, wall, and bridge, as shown in Figure 4(a). Given that the potential of L-S TENG as a future energy harvesting technology has been verified by various studies, it should move on to the next stage for practical application. On the other hand, outdoor conditions can cause easy and continuous weathering, wear, and contamination of the contact layer, which is the outermost one exposed to the outside. In this respect, the contact layer for L-S TENG is required in large areas and mass quantities for its facile and cost-effective replacement when environmental wear and contamination occurs because its frequently suggested applications include outdoor installation for harvesting raindrop energy, resulting in easy and continuous weathering. The working mechanism of L-S TENG, which generates electricity from the interaction between the liquid and solid surfaces, is illustrated in Figure 4(a). Given that one of the most critical factors affecting the output performance of L-S TENG is the hydrophobicity and hysteresis of the contact layer, which can facilitate the slip and detachment of the droplet, thus, polymeric contact layer with surface structures can improve the output performance of L-S TENG [45, 46]. In this respect, the polymeric contact layer with surface structures produced by a practical one-step rapid process based on the injection molding of fluoropolymers can be expected to play a key role in enhancing the electrical/practical performance of L-S TENG. The contact angles of the flat PFA contact layer, which has no surface structure, and a microcone-shaped structured PFA contact layer are shown in Figure 4(b) <i> and <ii>, respectively. As shown in the photographs, the flat PFA contact layer exhibits hydrophobic (contact angle of 105.2°) characteristics, whereas the surface-structured PFA contact layer exhibits superhydrophobic (contact angle of 155.1°) characteristics with the help of the presence of microstructures. In this study, the PFA contact layer with the microcone-shaped structure is applied for a subsequent parametric study. Figure 4(c) shows $V_{O,\max}$ depending on the concentration of the electrolyte solution (C). According to electrokinetic theory, the electrical output of L-S TENGs shows degradation with increasing C because the amount of electric charge (Q) generated from liquid-solid contact electrification is linearly proportional to zeta potential ζ, which is a widely used solid surface characteristic in the liquid-solid interface research field, as shown in the following relationship:

$$Q \propto \zeta \propto -\log C \equiv pC, \tag{3}$$

where pC is a similar concept to pH, which is the measure of hydrogen ions in an aqueous solution. In this respect, the generation behavior of $V_{O,\max}$, which is linearly proportional to pC, as shown in Figure 4(d), can support that the electrical output generated during the contact between the droplet and PFA contact layer is indeed based on the contact electrification between the liquid and solid surfaces. Figure S9 in the Supplementary Materials shows the analysis of the output performance characterization of L-S TENG with the injection-molded PFA contact layer by varying the angle between the falling droplet and contact layer (θ) by simulating the case where L-S TENG is installed in the roof. Figure S9(a) is the photograph captured by a high-speed camera of the moments that a droplet and tilted PFA contact layer come into contact when θ is 30, 45, 60, and 75°, and the contact areas in each case are measured, as shown in Figure S9(b). The contact area of the droplet and contact

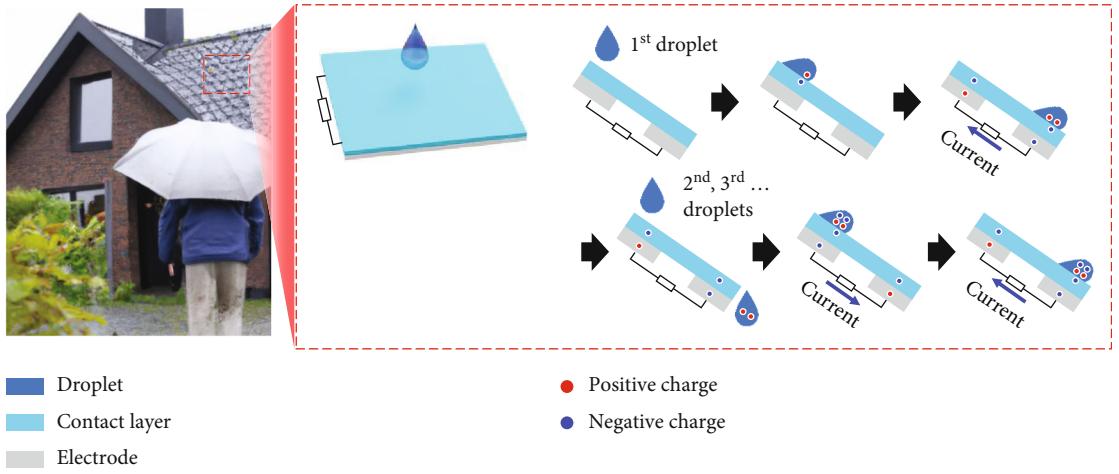

(a)

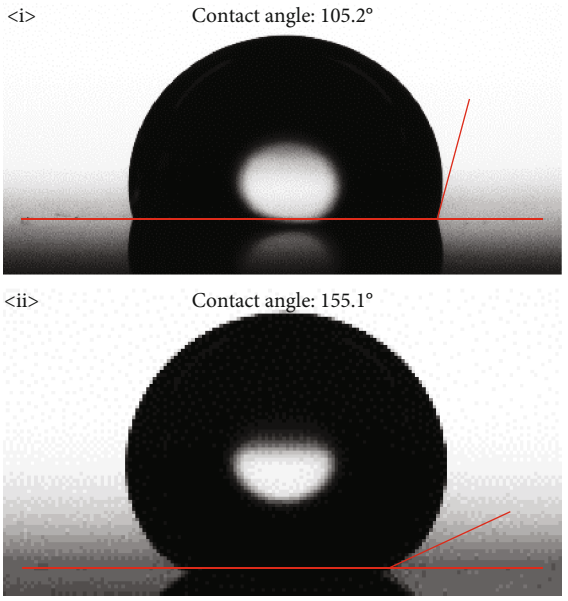

(b)

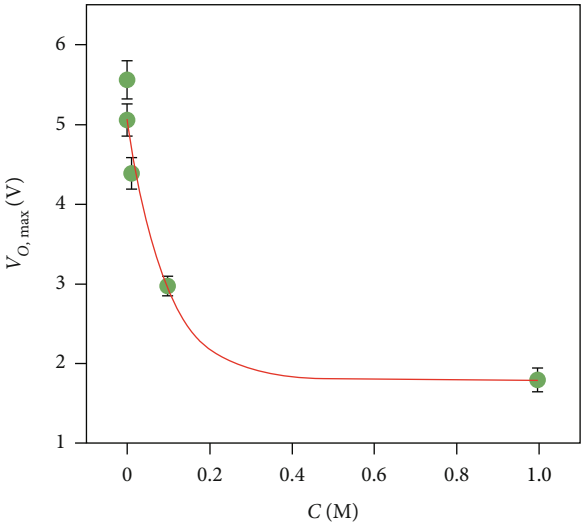

(c)

Figure 4: Continued.

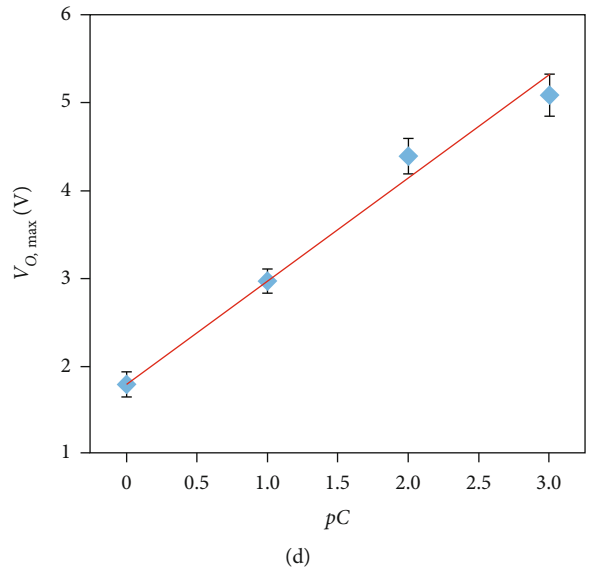

Figure 4: (a) A conceptual example of raindrop energy harvesting with L-S TENG and the working mechanism of the L-S TENG. (b) Contact angles of the flat surface PFA contact layer and the surface-structured PFA contact layer. $V_{O,\max}$ of the L-S TENG by varying (c) C and (d) pC.

layer increases with increasing θ because the droplet falls perpendicularly onto the contact layer and comes into contact with high impact. Based on the impacting dynamics of droplets on inclined surfaces, droplets falling from the same height with the same volume have a higher impact when they collide with the surface with increasing θ. The phenomenon that a droplet receiving a higher impact forms a wide contact area with a surface has been reported by several studies [47]. In this regard, this phenomenon is experimentally studied in this work and correlated with the electrical output performance of L-S TENG since the contact area is one of the major factors that can influence on electrical output performance of TENG. On the other hand, the hysteresis of the surface-structured PFA sheet is measured at 40°. Therefore, the droplet does not flow well when θ is too large, and the flow speed of the droplet on the injection-molded PFA contact layer in the case that θ is 75° is about 0 m/s, as shown in Figure S9(c). Considering the contact angle and hysteresis, the surface of the injection-molded PFA contact layer fabricated in this work is regarded as the superhydrophobic surface with the rose petal effect. Resultingly, when θ is 75°, the droplet that previously fell remains on the contact layer until the falling of the next droplet. This phenomenon causes a decrease in the effective contact between the droplet and the contact layer, and the electrical output of L-S TENG can decrease. Based on the above investigations, the change in the contact area and flow speed of the droplet is in a trade-off relationship depending on θ, and the electrical performance of L-S TENG can change. In this respect, the electrical output performance of L-S TENG according to θ is characterized, as shown in Figure S9(d).

3.4. Relationship between the Wear of the Surface Structure on the Contact Layer and the Electrical Output Performance of TENGs. The wear problem of the micro/nanoscale surface structures of polymeric contact layers is considered one of the most critical challenges in the field of TENGs with respect to practical application, although structured polymeric contact layers have been verified as one of the most appropriate contact layers of TENGs thanks to their electrical advantage as abovementioned. Prior to its quantitative investigation of the electrical output behavior by varying the wear rate of the surface structures, a TENG with an injection-molded PFA contact layer is operated until a noticeable degradation of the electrical output performance; the electrical output and SEM images before/after the operation of 24,000 cycles are shown in Figures 5(a)–5(c). The electrical output, which reached up to 540 V at the beginning of the operation, continuously decreased to about 350 V after 24,000 cycles of operation, as plotted in Figure 5(a). The surface structures of the contact layer are crushed, as shown in Figure 5(c) compared with the initial state (Figure 5(b)). As it can be recognized in this result, the crushing of the structures dominantly appeared as one of the various types of wear of surface structures on the contact layer of vertical contact separation operation mode-based TENG, and it may be related to the degradation of the electrical output performance. In order to quantitatively investigate the relationship between the crushing of surface structures and the output performance of TENGs, six PFA contact layers with different crushing degrees of the surface structures are prepared, as shown in Figure 5(d). To mimic the different crushing degrees of the surface structures quantitatively, the force (F) having different magnitudes for each sample is applied uniformly to the structured surface of the PFA contact layer. The magnitudes of F applied to the six prepared samples are 0, 4, 8, 12, 16, and 20 kN, respectively, as shown in Figure 5(d). Then, the electrical outputs generated by TENGs with the six contact layer samples are measured, as plotted in Figure 5(e). The experimental setup and parametric conditions are all the same as in the above experiments to confirm the effect of the difference in surface structure. The

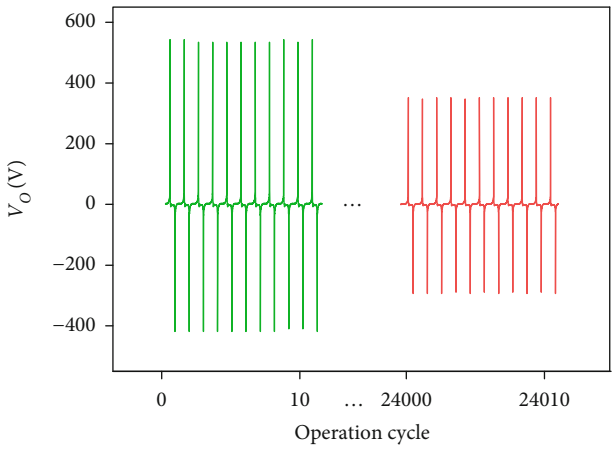

(a)

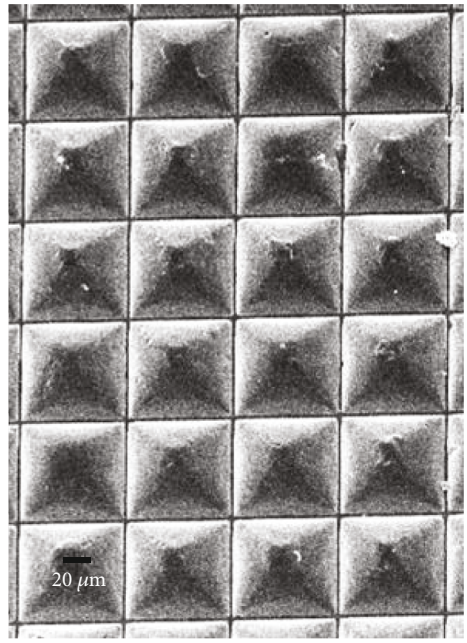

(b)

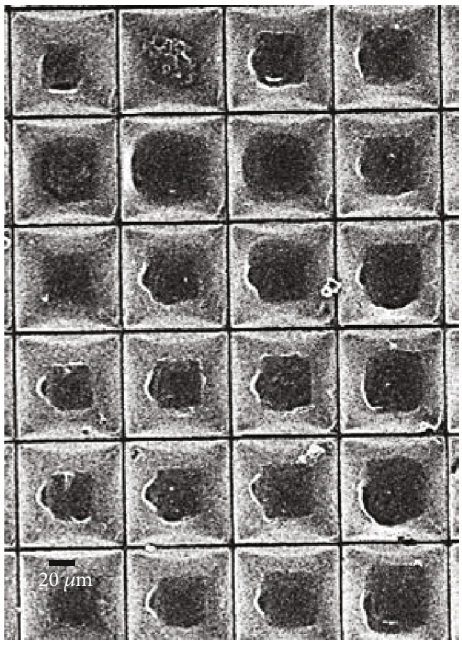

(c)

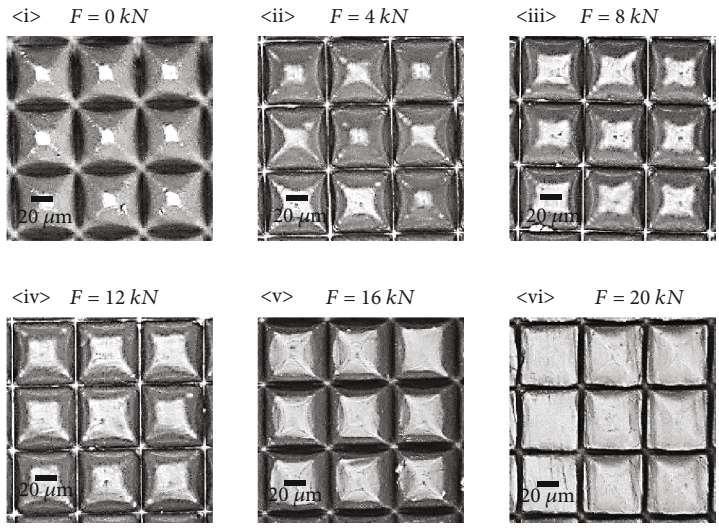

(d)

Figure 5: Continued.

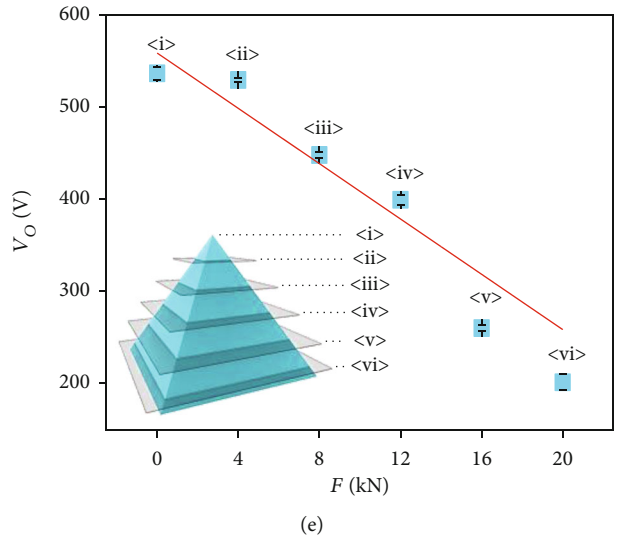

Figure 5: (a) Degradation of the electrical output performance of the TENG during a number of cycles of operation and SEM images of the contact surfaces of (b) the initial state and (c) after 24000 cycles of operation. (d) SEM images of the PFA contact layers with different crushed degrees of the surface structures and (e) the electrical outputs generated by the TENG with each contact layer.

inset schematically shows the degrees of crushing of the surface structures. As shown in the plot, the electrical output performance of the TENG is degraded with an increase in the degree of crushing of the surface structures on the contact layer. Compared with the result of the experiment in Figures 5(a)–5(c), the result of this experiment is reasonable because both the degree of crushing of the surface structures (Figure 5(c)) and the amount of reduced electrical output (Figure 5(a)) are between <iv> and <v> of Figures 5(d) and 5(e). Given all these experimental results, the crushing of the surface structures on the contact layer and the degradation of the electrical output performance of TENGs have a direct relationship with vertical contact separation mode-based TENGs. Moreover, when TENGs with an injection-molded PFA contact layer are operated for approximately 43,200 cycles on the basis of the vertical contact separation mode, the electrical output performance shows considerable degradation. As shown in this experimental result, the phenomenon of the decrease in electrical output due to the long-term operation-induced wear of the surface structure of the contact layer is an unavoidable problem when polymeric materials are used as the contact layer of TENGs. However, the injection-molded contact layer can give a solution, although it is not the direct troubleshooter, as the available and replaceable contact layer can be easily replaced since it can be manufactured with quantitatively and qualitatively reliable mass production.

3.5. Tile Floor-Based TENGs with Mass-Producible, Replaceable, and Fully Recyclable Contact Layers. In consideration of the working mechanism and wear characteristic of vertical contact separation mode-based TENGs based on the above investigations, a tile floor-based TENG with an injection-molded polymeric contact layer, which has microscale surface structures and is mass-produced via injection molding, is proposed as a proof-of-concept demonstration to show the potential and ability of injection-molded polymeric contact layers to be replaceable but fully recyclable (see concept art in Figure 6(a)). Figures 6(b) and 6(c) show photographs of the tile floor with PFA contact layers and the experimental setup with a TENG, respectively. The output performance generated from a tile floor-based TENG when a person walks and runs is plotted in Figure 6(c). Substantial biomechanical energy can be easily harvested from daily human movements, such as walking and running. Figure 6(d) shows the replaceability and recyclability of the proposed polymeric contact layer with surface structures produced based on the injection molding process, which are the strongest points of this work. When the electrical output performance is degraded after numerous operation cycles as shown in Figure 6(d) <i> and<ii> and related graphs, which should be mainly caused by the wear of the surface structures of the contact layer, the contact layer can be easily replaced with the available new one and the remanufactured one as shown in Figure 6(d) <iii> and <iv> because the contact layer can be mass produced via the low-cost injection molding process and the TENGs have a simple structure for the replacement. Then, the electrical output can be generated at the same level in the initial state as shown in Figure 6(d) <v>. Figure 6(d) <v> shows a photograph of the tile floor for which the replacement of worn tiles has been completed and its electrical output performance. Furthermore, the postused polymeric contact layers, which were produced by the injection molding process, can be fully recycled, as shown in Figure 6(d) <iii-1>, <iii-2>, <iii-3>, and <iii-4>. Contact layers are traditionally discarded when the surface structures are worn and the electrical output is degraded. By contrast, injection-molded PFA contact layers can be reprocessed as material for injection molding because they are thermoplastic, which can be melted and turned into resin by heating. As shown in Figure 6(d) <iii-1> and <iii-2>, after the worn PFA contact layers are collected and cleaned, they can be pelletized for injection molding. Then, new PFA contact layers with intact surface structures can be

(a)

(b)

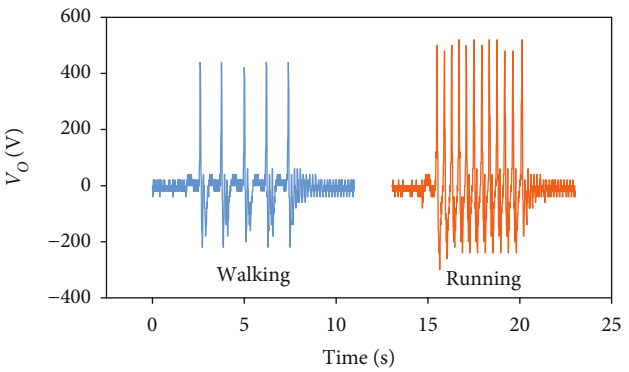

(c)

Figure 6: Continued.

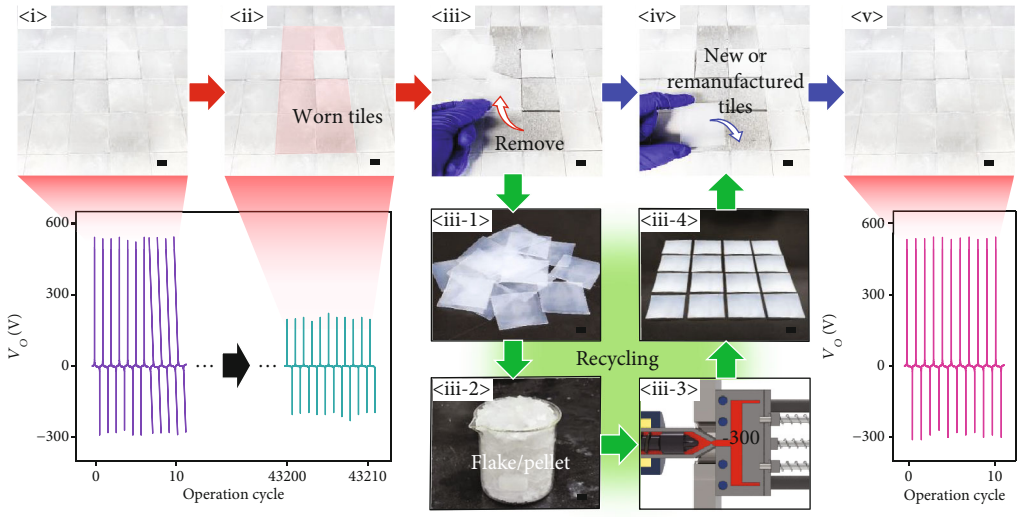

(d)

FIGURE 6: (a) Concept art and working mechanism of the tile floor-based TENG with the replaceable and recyclable polymeric contact layer. (b) Photographs of the tile floor with the PFA contact layers and experimental setup with TENG for the concept demonstration. (c) Output performance generated from the tile floor-based TENG when a person walks and runs. (d) Replaceability (<i>→<ii>→<iii>→<iv>→<v>) and recyclability (<iii-1>→<iii-2>→<iii-3>→<iii-4>) of the proposed surface-structured PFA contact layer for the TENG with the output performance of each case and its recovery. All scale bars are 1 cm.

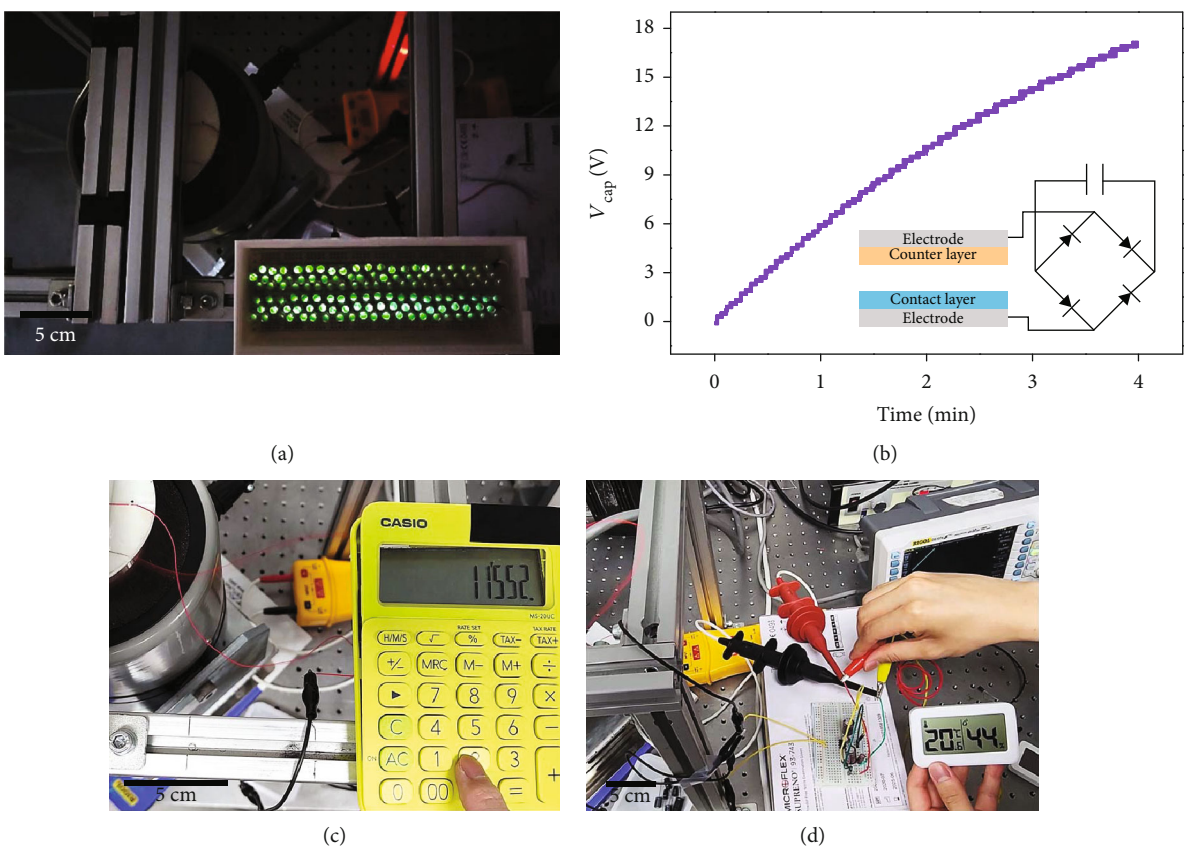

(a) (b)

(c) (d)

FIGURE 7: (a) Operation of LEDs by directly connecting the PFA contact layer introduced S-S TENG. (b) Charging behavior of a capacitor (10 μF) using S-S TENG. Driving (c) calculator and (d) thermohydrometer using the capacitor charged by S-S TENG.

remanufactured by injection molding, as shown in Figure 6(d) <iii-3> and <iii-4>. Figure 6(d) <iii-4> shows a photograph of remanufactured polymeric contact layers. Given that, injection-molded PFA contact layers can be produced and fully recycled through a closed-loop supply chain. Furthermore, considering that polymeric contact layers are the part that wears out the most in TENGs, zero-waste manufacturing of polymeric contact layers can help TENGs be utilized as semipermanent and ecofriendly energy harvesters.

3.6. Operation of Electronic Devices Using TENG including the Surface-Structured PFA Contact Layer. TENG can be introduced as a power source for driving various electronic devices. The harvested mechanical energy using the manufactured PFA contact layer-included TENG can be utilized as electrical energy, and it can produce electricity in both direct and indirect ways for electronic devices, as shown in Figure 7. Figure 7(a) shows the operation of hundreds of light-emitting diodes (LEDs) by directly connecting the PFA contact layer introduced by S-S TENG. The PFA contact layer has a cone-shaped surface structure. The contact area is 5 cm × 5 cm, and the contact frequency is 10 Hz, as in the above experiments. Figure 7(b) shows the charging behavior of a capacitor (10 μF) that is charged using S-S TENG. The capacitor can be charged over 15 V within 3 min of operating S-S TENG. Figures 7(c) and 7(d) are photographs of the driving calculator and thermohydrometer using the capacitor that is charged by S-S TENG. Given that, TENG with the surface-structured PFA contact layer manufactured by the injection molding process can be applied to driving various electronic devices and supplying electricity for charging a capacitor.

4. Conclusion

In this study, injection molding-assisted mass production of polymeric contact layers with surface structures is proposed. Given that the surface structure of polymeric contact layers plays a key role in the generation of electricity in TENGs, the wear-induced limited lifetime of surface structures is one of the most critical challenges hindering the commercialization of TENGs. In this respect, injection molding is introduced to mass-produce surface-structured polymeric contact layers, and surface-structured polymeric contact layers can be reliably manufactured. On the basis of the wear characteristics of polymeric contact layers and the working mechanism of TENGs, a tile floor-based TENG with an injection-molded PFA contact layer is developed, and the replaceability and recyclability of the contact layer are demonstrated. Although only the vertical contact separation mode-based TENG is demonstrated as an application in this study, the advantageous replaceability and recyclability of injection-molded polymeric contact layers can contribute to, including but not limited to, vertical contact separation mode-based TENGs. The wear issue, including abrasive wear, fatigue wear, and corrosion wear, of the contact layer is one of the most critical challenges in various types of TENGs, such as rotational, fluttering, cylindrical, and sliding TENGs. Given that, injection molding-assisted mass production of contact layers is expected to broaden the applicability of various TENGs as semipermanent and ecofriendly energy harvesters.

Data Availability

The data used to support the findings of this study are available upon request from the authors.

Conflicts of Interest

The authors declare that they have no conflicts of interest.

Authors' Contributions

Y. Ra and J. H. Lee contributed equally to this work.

Acknowledgments

This work was supported by the Human Resources Development of the Korea Institute of Energy Technology Evaluation and Planning (KETEP) grant funded by the Korea government Ministry of Knowledge Economy (No. RS-2023-00244330). This work was partly supported by the Technology Development Program of MSS (S2959724). This study has been conducted with the support of the Korea Institute of Industrial Technology as "Development of intelligent root technology with add-on modules (KITECH EO-22-0005)".

Supplementary Materials

Optimization of the condition of the injection molding process is explained. Concise descriptions of figures and tables in Supplementary Materials are as follows. Figure S1: diamond turning machining (DTM) and electroforming process for fabricating the mold insert block. Figure S2: (a) change of the surface topography of the injection-molded PFA contact layers and (b) S/N ratio in the optimization of the injection molding process. Figure S3: photographs and surface topographies of the mold inserts with three types of negative surface structures ((a) microcone shape, (b) microsquare pillar shape, and (c) microsquare pyramid shape). Figure S4: (a) photograph of the experimental setup for the operation of S-S TENG. (b) S-S TENG mounted on the shaker. The inset is a photograph of the PFA contact layer and APTES counter layer with aluminum electrodes. Figure S5: gradual increase and saturation of electrical output of S-S TENG with its continuous operation. Figure S6: power density generated by S-S TENG by varying the external load resistance. Figure S7: electrical output performance of S-S TENG with the injection-molded PFA contact layer according to the relative humidity. Figure S8: output voltage of S-S TENG when the (a) PLA and (b) PVA sheets are used as the contact layer. Figure S9: (a) photographs captured by a high-speed camera of the moments that a droplet and tilted PFA contact layer come into contact when θ is <i> 30, <ii> 45, <iii> 60, and <iv> 75°. (b) Contact area, (c) flow speed, and (d) electrical output of L-S TENG depending on θ. Table S1: parameter design for injection molding. Table S2: design of experiments (orthogonal arrays of $L_9 3^4$). Table S3:

processing conditions applied to the injection molding process for the replication of PFA contact layers. Table S4: cost of the injection molding process for manufacturing the PFA contact layers. *(Supplementary Materials)*

References

[1] D. Heo, M. Song, S.-H. Chung et al., "Inhalation-driven vertical flutter triboelectric nanogenerator with amplified output as a gas-mask-integrated self-powered multifunctional system," *Advanced Energy Materials*, vol. 12, no. 31, article 2201001, 2022.

[2] H. Joo, K. Y. Lee, and J.-H. Lee, "Piezo/triboelectric effect driven self-powered gas sensor for environmental sensor networks," *Energy Technology*, vol. 10, no. 7, 2022.

[3] J. Chung, D. Heo, K. Cha, Z.-H. Lin, J. Hong, and S. Lee, "A portable device for water-sloshing-based electricity generation based on charge separation and accumulation," *Iscience*, vol. 24, no. 5, article 102442, 2021.

[4] C. Xu, Y. Song, M. Han, and H. Zhang, "Portable and wearable self-powered systems based on emerging energy harvesting technology," *Microsystems & Nanoengineering*, vol. 7, no. 1, pp. 1–14, 2021.

[5] K. Cha, J. Chung, D. Heo et al., "Lightweight mobile stick-type water-based triboelectric nanogenerator with amplified current for portable safety devices," *Science and Technology of Advanced Materials*, vol. 23, no. 1, pp. 161–168, 2022.

[6] P. M. R. Carneiro, J. V. Vidal, P. Rolo et al., "Instrumented electromagnetic generator: optimized performance by automatic self-adaptation of the generator structure," *Mechanical Systems and Signal Processing*, vol. 171, article 108898, 2022.

[7] Y. Ra, J. Kim, H. Kim et al., "Smart conveyor roller system for self-powered product size identification in electrically off-grid condition via hybridization of triboelectric-electromagnetic generators," *Nano Energy*, vol. 100, article 107447, 2022.

[8] S. Sharma, R. Kiran, P. Azad, and R. Vaish, "A review of piezoelectric energy harvesting tiles: available designs and future perspective," *Energy Conversion and Management*, vol. 254, article 115272, 2022.

[9] Y. Ra, J. H. Choi, S.-J. Choi et al., "Cold rolled robust metal assisted triboelectric nanogenerator for extremely durable operation," *Extreme Mechanics Letters*, vol. 40, article 100910, 2020.

[10] Y. Yun, M. La, S. Cho, and S. Jang, "High quality electret based triboelectric nanogenerator for boosted and reliable electrical output performance," *International Journal of Precision Engineering and Manufacturing-Green Technology*, vol. 8, no. 1, pp. 125–137, 2021.

[11] D. Lee, S. Cho, S. Jang et al., "Toward effective irregular wind energy harvesting: self-adaptive mechanical design strategy of triboelectric-electromagnetic hybrid wind energy harvester for wireless environmental monitoring and green hydrogen production," *Nano Energy*, vol. 102, article 107638, 2022.

[12] S. Cho, Y. Yun, S. Jang et al., "Universal biomechanical energy harvesting from joint movements using a direction-switchable triboelectric nanogenerator," *Nano Energy*, vol. 71, article 104584, 2020.

[13] S. Choi, S. Cho, Y. Yun et al., "Development of a high-performance handheld triboelectric nanogenerator with a lightweight power transmission unit," *Advanced Materials Technologies*, vol. 5, no. 4, article 2000003, 2020.

[14] S. Jang, M. La, S. Cho et al., "Monocharged electret based liquid-solid interacting triboelectric nanogenerator for its boosted electrical output performance," *Nano Energy*, vol. 70, article 104541, 2020.

[15] D. Yoo, S. Lee, J.-W. Lee et al., "Reliable DC voltage generation based on the enhanced performance triboelectric nanogenerator fabricated by nanoimprinting-poling process and an optimized high efficiency integrated circuit," *Nano Energy*, vol. 69, article 104388, 2020.

[16] P. Chen, Y. Luo, R. Cheng et al., "Achieving high power density and durability of sliding mode triboelectric nanogenerator by double charge supplement strategy," *Advanced Energy Materials*, vol. 12, no. 33, article 2201813, 2022.

[17] D.-M. Lee, N. Rubab, I. Hyun et al., "Ultrasound-mediated triboelectric nanogenerator for powering on-demand transient electronics," *Science Advances*, vol. 8, no. 1, article eabl8423, 2022.

[18] Z. Ren, L. Wu, Y. Pang, W. Zhang, and R. Yang, "Strategies for effectively harvesting wind energy based on triboelectric nanogenerators," *Nano Energy*, vol. 100, article 107522, 2022.

[19] Y. Wu, Y. Li, Y. Zou et al., "A multi-mode triboelectric nanogenerator for energy harvesting and biomedical monitoring," *Nano Energy*, vol. 92, article 106715, 2022.

[20] J. H. Choi, Y. Ra, S. Cho, M. La, S. J. Park, and D. Choi, "Electrical charge storage effect in carbon based polymer composite for long-term performance enhancement of the triboelectric nanogenerator," *Composites Science and Technology*, vol. 207, article 108680, 2021.

[21] L. Liu, J. Li, W. Ou-Yang et al., "Ferromagnetic-assisted Maxwell's displacement current based on iron/polymer composite for improving the triboelectric nanogenerator output," *Nano Energy*, vol. 96, article 107139, 2022.

[22] G. Lu, C. Huang, M. Qiu et al., "Output enhancement of triboelectric nanogenerators based on hierarchically regular cadmium coordination polymers for photocycloaddition," *Inorganic Chemistry*, vol. 61, no. 32, pp. 12736–12745, 2022.

[23] C. Xing, Y. Tian, Z. Yu, B. Meng, and Z. Peng, "Cellulose nanofiber-reinforced MXene membranes as stable friction layers and effective electrodes for high-performance triboelectric nanogenerators," *ACS Applied Materials & Interfaces*, vol. 14, no. 32, pp. 36741–36752, 2022.

[24] X. Yu, J. Ge, Z. Wang, J. Wang, Z. L. W. Da Zhao, and T. Cheng, "High-performance triboelectric nanogenerator with synchronization mechanism by charge handling," *Energy Conversion and Management*, vol. 263, article 115655, 2022.

[25] I.-W. Tcho, W.-G. Kim, S.-B. Jeon et al., "Surface structural analysis of a friction layer for a triboelectric nanogenerator," *Nano Energy*, vol. 42, pp. 34–42, 2017.

[26] S. Cho, S. Jang, M. La, Y. Yun, and T. Yu, "Facile tailoring of contact layer characteristics of the triboelectric nanogenerator based on portable imprinting device," *Materials*, vol. 13, no. 4, p. 872, 2020.

[27] M. Ibrahim, J. Jiang, Z. Wen, and X. Sun, "Surface engineering for enhanced triboelectric nanogenerator," *Nanoenergy Advances*, vol. 1, no. 1, pp. 58–80, 2021.

[28] Y. Sun, Y. Zheng, R. Wang et al., "3D micro-nanostructure based waterproof triboelectric nanogenerator as an outdoor adventure power source," *Nano Energy*, vol. 100, article 107506, 2022.

[29] H. Zhang, P. Zhang, D. Lu, and X. Fan, "Enhancement of triboelectric nanogenerators output performance by background

paper-based hierarchical micro-structures for energy harvesting," *Applied Physics Letters*, vol. 121, no. 6, article 063902, 2022.

[30] G. Zhu, B. Peng, J. Chen, Q. Jing, and Z. Lin Wang, "Triboelectric nanogenerators as a new energy technology: from fundamentals, devices, to applications," *Nano Energy*, vol. 14, pp. 126–138, 2015.

[31] C. Wu, A. C. Wang, W. Ding, H. Guo, and Z. L. Wang, "Triboelectric nanogenerator: a foundation of the energy for the new era," *Advanced Energy Materials*, vol. 9, no. 1, p. 1802906, 2019.

[32] M. A. P. Mahmud, A. Zolfagharian, S. Gharaie et al., "3D-printed triboelectric nanogenerators: state of the art, applications, and challenges," *Advanced Energy and Sustainability Research*, vol. 2, no. 3, article 2000045, 2021.

[33] Z. B. Li, H. Y. Li, Y. J. Fan et al., "Small-sized, lightweight, and flexible triboelectric nanogenerator enhanced by PTFE/PDMS nanocomposite electret," *ACS Applied Materials & Interfaces*, vol. 11, no. 22, pp. 20370–20377, 2019.

[34] A. Chen, C. Zhang, G. Zhu, and Z. L. Wang, "Polymer materials for high-performance triboelectric nanogenerators," *Advanced Science*, vol. 7, no. 14, p. 2000186, 2020.

[35] S. Han, E. J. Lee, B. Kim et al., "High-performance dual-mode triboelectric nanogenerator based on hierarchical auxetic structure," *ACS Energy Letters*, vol. 5, no. 11, pp. 3507–3513, 2020.

[36] Y. Ra, O. Seungin, J. H. Lee et al., "Triboelectric signal generation and its versatile utilization during gear- based ordinary power transmission," *Nano Energy*, vol. 73, article 104745, 2020.

[37] M. Kim, Y. Ra, S. Cho et al., "Geometric gradient assisted control of the triboelectric effect in a smart brake system for self-powered mechanical abrasion monitoring," *Nano Energy*, vol. 89, p. 106448, 2021.

[38] H. Teng, "Overview of the development of the fluoropolymer industry," *Applied Sciences*, vol. 2, no. 2, pp. 496–512, 2012.

[39] J. Gardiner, "Fluoropolymers: origin, production, and industrial and commercial applications," *Australian Journal of Chemistry*, vol. 68, no. 1, pp. 13–22, 2015.

[40] D. Znidar, D. Dallinger, and C. O. Kappe, "Practical guidelines for the safe use of fluorine gas employing continuous flow technology," *ACS Chemical Health & Safety*, vol. 29, no. 2, pp. 165–174, 2022.

[41] Z. Qin, Y. Yin, W. Zhang, C. Li, and K. Pan, "Wearable and stretchable triboelectric nanogenerator based on crumpled nanofibrous membranes," *ACS Applied Materials & Interfaces*, vol. 11, no. 13, pp. 12452–12459, 2019.

[42] C. Pinming, W. Wongwiriyapan, S. Rattanamai et al., "Carbon nanotube/polydimethylsiloxane composite micropillar arrays using non-lithographic silicon nanowires as a template for performance enhancement of triboelectric nanogenerators," *Nanotechnology*, vol. 32, no. 9, article 095303, 2021.

[43] Y. Zou, J. Xu, K. Chen, and J. Chen, "Advances in nanostructures for high-performance triboelectric nanogenerators," *Advanced Materials Technologies*, vol. 6, no. 3, article 2000916, 2021.

[44] B. Fan, G. Liu, F. Xianpeng, Z. Wang, Z. Zhang, and C. Zhang, "Composite film with hollow hierarchical silica/perfluoropolyether filler and surface etching for performance enhanced triboelectric nanogenerators," *Chemical Engineering Journal*, vol. 446, article 137263, 2022.

[45] D. Choi and D. Yoo, "Spontaneous occurrence of liquid-solid contact electrification in nature: toward a robust triboelectric nanogenerator inspired by the natural lotus leaf," *Nano Energy*, vol. 36, pp. 250–259, 2017.

[46] H. Cho, J. Chung, G. Shin et al., "Toward sustainable output generation of liquid–solid contact triboelectric nanogenerators: the role of hierarchical structures," *Nano Energy*, vol. 56, pp. 56–64, 2019.

[47] J.-M. Tian and B. Chen, "Dynamic behavior of non-evaporative droplet impact on a solid surface: comparative study of R113, water, ethanol and acetone," *Experimental Thermal and Fluid Science*, vol. 105, pp. 153–164, 2019.